

# Journal of Materials Chemistry A

Materials for energy and sustainability

Accepted Manuscript

This article can be cited before page numbers have been issued, to do this please use: S. Dey, D. Langgut, T. Gutmann, Z. Kelemen, R. Pietschnig and B. Szathmári, *J. Mater. Chem. A*, 2026, DOI: 10.1039/D6TA02261H.



This is an Accepted Manuscript, which has been through the Royal Society of Chemistry peer review process and has been accepted for publication.

Accepted Manuscripts are published online shortly after acceptance, before technical editing, formatting and proof reading. Using this free service, authors can make their results available to the community, in citable form, before we publish the edited article. We will replace this Accepted Manuscript with the edited and formatted Advance Article as soon as it is available.

You can find more information about Accepted Manuscripts in the [Information for Authors](#).

Please note that technical editing may introduce minor changes to the text and/or graphics, which may alter content. The journal's standard [Terms & Conditions](#) and the [Ethical guidelines](#) still apply. In no event shall the Royal Society of Chemistry be held responsible for any errors or omissions in this Accepted Manuscript or any consequences arising from the use of any information it contains.

# Metallopolymers via Thermal Dealkylation of Unstrained Bisphosphanylferrocene Precursors

View Article Online  
DOI: 10.1039/D6TA02261H

Subhayan Dey,\*<sup>a, b</sup> Balázs Szathmári,<sup>c</sup> Dennis Langgut,<sup>a</sup> Torsten Gutmann,\*<sup>d, e</sup> Zsolt Kelemen,\*<sup>c</sup> Rudolf Pietschnig\*<sup>a</sup>

a. Institut für Chemie und CINSaT, University of Kassel, Heinrich-Plett-Straße 40, 34132 Kassel, Germany. E-mail: [pietschnig@uni-kassel.de](mailto:pietschnig@uni-kassel.de)

b. Department of Chemistry, School of Advanced Sciences, Vellore Institute of Technology, Vandalur-Kelambakkam Road, Keelakotaiyur, Chennai, Tamil Nadu 600127, India. E-mail: [subhayan.dey@vit.ac.in](mailto:subhayan.dey@vit.ac.in)

c. Department of Inorganic and Analytical Chemistry, Faculty of Chemical Technology and Biotechnology, Budapest University of Technology and Economics, Műgyetem rkp 3, 1111, Budapest, Hungary. E-mail: [kelemen.zsolt@vbk.bme.hu](mailto:kelemen.zsolt@vbk.bme.hu)

d. Department of Chemistry, Paderborn University, Warburger Str. 100, 33098 Paderborn, Germany. E-mail: [torsten.gutmann@uni-paderborn.de](mailto:torsten.gutmann@uni-paderborn.de)

e. Institute of Inorg. and Phys. Chemistry, TU Darmstadt, Peter-Grünberg-Str. 8, 64287 Darmstadt, Germany

## Abstract

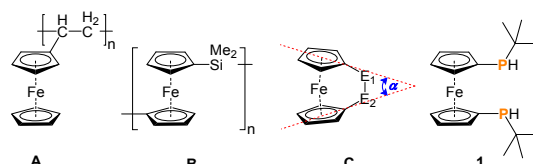
Ferrocenylene-bridged polyphosphanes  $[\text{Fc}'\text{P}_2]_n\text{tBu}_2$  and  $[\text{Fc}'\text{P}_2]_n$  ( $\text{Fc}' = 1,1'$ -ferrocenediyl;  $\text{tBu} = \textit{tert}$ -butyl) previously prepared via thermal ring expansion polymerization from strained ferrocenophane precursors, are reported to be accessible from unstrained secondary phosphanes. Thermal reaction and polymerization of  $\text{Fe}(\text{C}_5\text{H}_4\text{-PHtBu})_2$  proceed through the elimination of  $\text{tBuH}$ , and consequent formation of  $\text{tBu}$ -substituted diphospha[2]FCP, along with ferrocene substituted cyclic  $\text{P}_4$ -species, and di- $\text{tBu}$ -substituted linear  $\text{P}_4$ -species. The resulting polymer shows similar  $^{13}\text{C}$  and  $^{31}\text{P}$  solid-state NMR, IR, and UV-Vis spectra, as well as elemental analyses, when compared to those of authentic samples of previously published  $[\text{Fc}'\text{P}_2]_n\text{tBu}_2$  and  $[\text{Fc}'\text{P}_2]_n$  obtained via strained ferrocenophanes. On the contrary, thermal reaction of all- $\text{tBu}$ -substituted tertiary phosphane  $\text{Fc}'(\text{P}^{\text{tBu}})_2$  entails loss of the P-containing moiety along with formation of  $\text{Fc}'\text{tBu}$  instead of polymeric material. Thermodynamic assessment of the decomposition pathways of both precursors based on density functional theory calculations is consistent with the experimental findings. Overall, the unstrained 1,1'-ferrocenylene bridged secondary bisphosphane provides a simplified approach for thermal polymerization to linear one-dimensional  $\text{P}_n$ -chains.

## 1. Introduction

Inorganic polymers offer remarkable upgradation in properties (e.g. higher decomposition temperature, lower flammability, lower glass transition temperature, etc.) compared with organic polymers.<sup>1</sup> They frequently consist of a handful of main-group elements, such as P, N, B, S, Si etc. (e.g. cyclo- and polyphosphazenes and their polymers, polyborazines, polythiophosphazenes, polysilanes, polysiloxanes etc.).<sup>2, 3</sup> Similarly, polymers with organometallic moieties as sidechain (i.e. pendant polymer **A**, Figure 1) or as part of the backbone (i.e. mainchain polymer **B**, Figure 1) are especially attractive owing to unique properties such as reversible redox properties in the case of ferrocene allowing for switchable or adaptive materials.<sup>4, 5</sup>

While ferrocene-based sidechain polymers (**A**, Figure 1) are commonly synthesized by polymerization of precursors with a polymerizable unit attached to ferrocene (e.g. vinyl group),<sup>4, 6, 7</sup> main-chain polymers (**B**, Figure 1) are commonly synthesized via directed ring-opening polymerization reactions (ROPs) of strained ferrocenophane (FCP) rings (**C**, Figure 1),<sup>8</sup> where the dihedral angle  $\alpha$  may be used to estimate the ring-strain in the molecule.<sup>9, 10</sup>

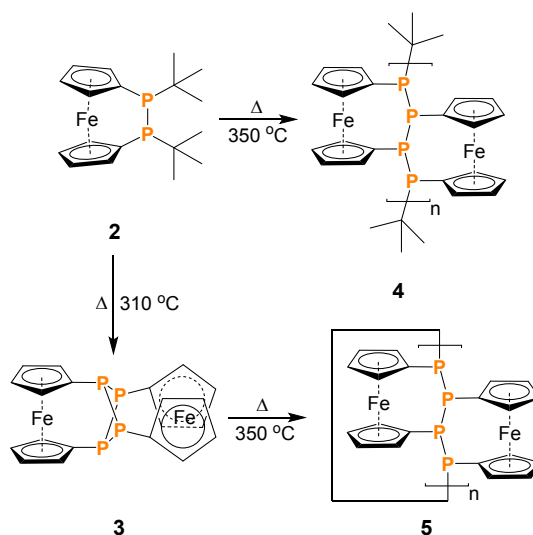




View Article Online  
DOI: 10.1039/D6TA02261H

**Fig 1.** Prominent examples of ferrocene containing sidechain (**A**);<sup>11</sup> and mainchain polymers (**B**).<sup>12</sup> General sketch of precursors, a strained ferrocenophane ( $E =$  organoelement fragment,  $\alpha =$  dihedral or tilt angle) (**C**);<sup>8</sup> and unstrained 1,1'-disubstituted ferrocene bisphosphane (**1**) used in this work.

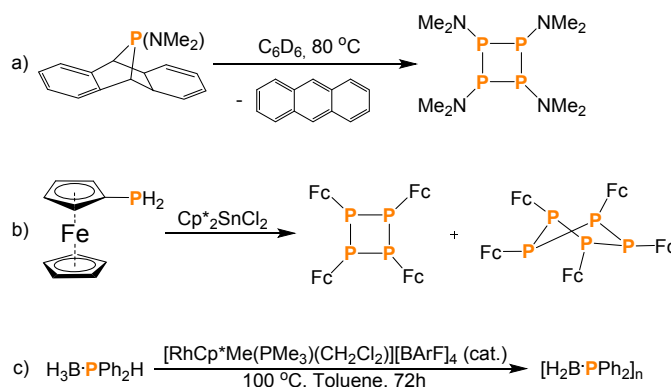
Recently,<sup>5, 8</sup> we have introduced a synthetic approach to oligo-/polymeric 1D- phosphorus chains **4** with ferrocenylene-bridges,<sup>13</sup> using ring expansion polymerization (REP) which employs thermal P-C dissociation and ring-opening of a diphospha[2]FCP **2** (Scheme 1).<sup>14</sup> In the course of this REP sequence a tetracyclic tetraphosphane intermediate **3** could be identified (Scheme 1) which has been fully characterized upon preparation via an independent synthetic route using salt metathesis under mild conditions.<sup>15</sup> Consistent with its role as central intermediate in the above mentioned REP, samples of isolated **3** are transformed into ferrocenylene-bridged polyphosphane metallopolymer (**5**) thermally (Scheme 1).<sup>15</sup>



**Scheme 1.** Thermal ring-expansion polymerization of phospho[2]FCP (**2**), via formation of tetracyclic tetraphosphane with twofold FCP bridges (**3**).

It is noteworthy that polymerization reactions via elimination of the small molecules have received significant attention. In particular, transition-metal catalyzed dehydrocoupling routes have been established for the preparation of polymers with inorganic backbones, such as Si-Si,<sup>16</sup> Ge-Ge,<sup>17</sup> Sn-Sn,<sup>18</sup> P-B,<sup>19</sup> and Si-O<sup>20</sup>. Catalytic dehydrocoupling involving pnictogens has been successfully utilized to access challenging products.<sup>21-23</sup> In this vein, dehydrocoupling reactions of primary phosphines received particular attention using heat (Scheme 2a),<sup>24</sup> or chemical reagents (e.g.  $Cp^*_2SnCl_2$  (Scheme 2b),<sup>25</sup> N-heterocyclic carbenes etc.<sup>26</sup>) to drive polymerization.<sup>27</sup> On the other hand, the dehydrocoupling of secondary phosphines has almost exclusively been achieved in the presence of transition metal catalysts for a few specific starting materials like phosphine boranes (Scheme 2c).<sup>28-30</sup> To the best of our knowledge, no precedence of thermal polymerization via dealkylation of secondary phosphines is available in the literature.





**Scheme 2.** Thermally (a)<sup>24</sup> or chemically driven (b),<sup>25</sup> and catalytic (c)<sup>28</sup> dehydropolymerization of primary and secondary phosphanes, where Fc stands for 1-ferrocenyl unit.

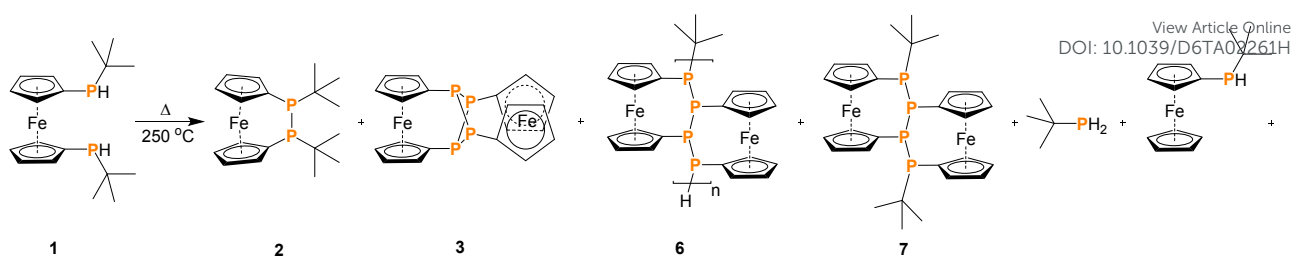
In the light of facile thermal P-C and P-P activation, during REP employing moderate to low strained precursors,<sup>13, 15</sup> we set out to investigate thermal reactions of their unstrained open-chain counterpart **1** as starting materials (Figure 1). The thus-obtained solid materials have been compared with authentic samples of the previously reported polymers **4** and **5** including solid-state NMR.<sup>13, 15</sup> To obtain an insight into thermodynamic and mechanistic aspects of the polymerization, we employed density functional theory (DFT), for interpretation of the experimentally obtained results.

## 2. Results and Discussions

The previously reported thermal cleavage of P-C and P-P bonds at elevated temperatures (i.e.  $310\text{ }^\circ\text{C}$  and  $335\text{ }^\circ\text{C}$ ) on a moderately strained and a virtually unstrained [2]- and [3]FCP (**2** and **3**, respectively) inspired us to investigate the scope of similar reaction on a truly unstrained secondary phosphane. Hydrogen and *tert*-butyl substituted **1** was chosen as potentially suitable starting material, as it can be obtained via a well-established synthetic protocol as an air stable compound,<sup>31</sup> owing to the presence of the ferrocene unit.<sup>32</sup> For the combination of hydrogen and *tert*-butyl groups as substituents at the phosphanyl groups, formation of an easily removable volatile byproduct (such as *tert*-butane) can be anticipated. To explore the dissociative polymerization, compound **1** was placed at high vacuum in a sealed glass ampule and subsequently heated from room temperature to  $250\text{ }^\circ\text{C}$  with a step-wise increase by  $10\text{ }^\circ\text{C}$  maintaining the conditions of each step unchanged for 1 h. After observing a prominent change in viscosity at ca.  $240\text{ }^\circ\text{C}$ , the reaction temperature was maintained at  $250\text{ }^\circ\text{C}$  for 4 hrs. Upon cooling the reaction ampule to room temperature, the semi-solid brown substance was extracted in  $C_6D_6$ , which upon investigation with liquid NMR spectroscopy showed a mixture of P-P coupled products besides unreacted **1** (doublet at  $\delta$  -27.10 ppm),  $FcP^tBuH$  (singlet at  $\delta$  -26.64 ppm), and  $^tBuPH_2$  (singlet at  $\delta$  -80.31 ppm) (Scheme 3 and Figure 2). The P-P coupled products have been identified as diphospha[2]FCP **2** (singlet at  $\delta$  20.43 ppm), ferrocene substituted cyclic  $P_4$ -species **3** (singlet at  $\delta$  39.10 ppm) and  $^tBu$ -substituted linear  $P_4$ -species **7** (multiplets at  $\delta$  -41.63 and 3.57 ppm). The identity of by-products **2**, **3** and **7** indicates successful P-C bond activation with elimination of the alkyl unit at phosphorus, as intended.

Removal of the low molecular by-products from the product mixture via repeated extraction with toluene and pentane, followed by drying under reduced pressure ( $10^{-3}$  mbar), affords the actual product **6** as an intractable solid which was characterized with solid-state NMR, IR spectroscopy and elemental analysis.





**Scheme 3.** Thermal reactions of **1**.

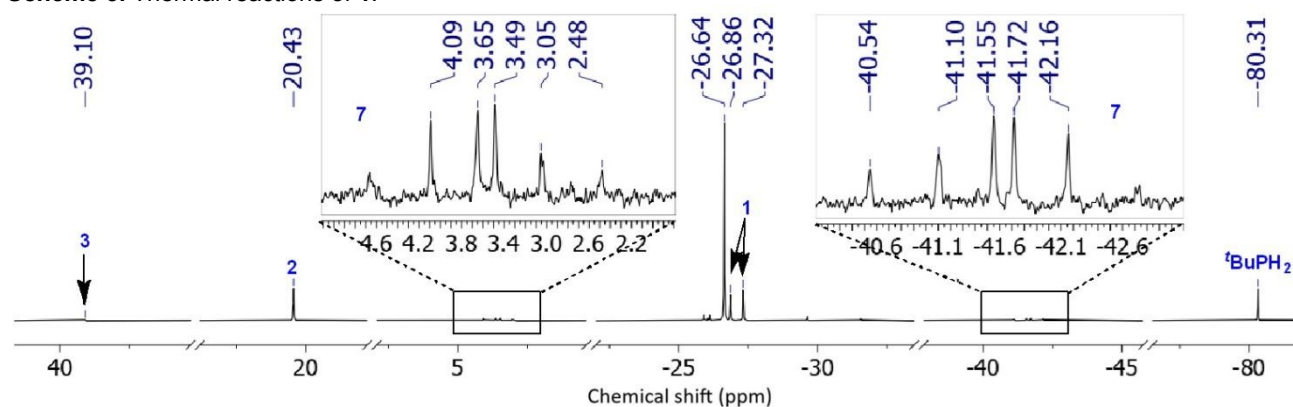


**Fig 2.**  $^{31}\text{P}$   $^{33}\text{NMR}$  (in  $\text{C}_6\text{D}_6$ ) spectrum of the soluble product from thermal polymerization of **1**, where the singlet at  $\delta$  -26.64 ppm is resulting from  $\text{FcP}'\text{BuH}$ .

For identification of structural units in compound **6**, solid-state NMR measurements have been performed. The  $^1\text{H} \rightarrow ^{31}\text{P}$  CP MAS NMR spectrum of **6** (Figure 3B) shows a pattern of few broad  $^{31}\text{P}$  resonances centered around  $\delta$  -8, -20 and -26 ppm reminiscent of those observed for closely related polymers **4** and **5**, which have been prepared from strained precursors.<sup>13, 15, 18</sup> For detailed comparison of polymer **6** with the previously reported analogous polymer **5**, an authentic sample of **5** was characterized with  $^1\text{H} \rightarrow ^{31}\text{P}$  CP MAS NMR spectroscopy at otherwise identical conditions (Figure 3A). By direct comparison, the  $^1\text{H} \rightarrow ^{31}\text{P}$  CP MAS NMR signatures of **5** and **6** match closely, and are consistent with chemically equivalent phosphorus centres in the backbone. It is also noteworthy that the above mentioned  $^{31}\text{P}$  resonances at  $\delta$  -8, -20 and -26 ppm for **5** and **6** are in good agreement with solid-state NMR data obtained for *o*-phenylene bridged (macro)cyclic cyclopolyphosphanes, reported by Woollins *et al* ( $\delta$  ( $^{31}\text{P}$ ) = -21.8 ppm),<sup>34</sup> and for **4**, reported by us ( $^{31}\text{P}$   $\delta$  -10 (CpP(*t*Bu)P<) and -24 ppm (P(P<)).<sup>13</sup> While related short chain oligomers in solution feature well resolved higher order spin systems, the *J*-couplings are not resolved in the above mentioned solid-state NMR spectra, as expected.

To overcome the limitations imposed by line broadening and to analyze scalar couplings in the solid-state, we also measured  $^{31}\text{P}$  J-resolved solid state  $^{31}\text{P}$  NMR spectra of **5** and **6**. As a result,  $^{31}\text{P}$ - $^{31}\text{P}$  couplings with ca. 290 Hz were observed in both cases for the main signals resonating at  $\delta$  -8, -20 and -26 ppm (Figures 3C and 3D). Further couplings in the order of 140 and 550 Hz are detectable for the signal appearing at ca.  $\delta$  -8 -20 and -26 ppm, for polymers **5** and **6**, respectively. Clearly scalar couplings reflect the *s*-character of the respective bond path and are strongly dependent on the angular geometry. It is here noteworthy that these couplings are smaller or larger than those found for the phosphanes in *trans*-position of Wilkinsons catalyst, featuring a value of ca. 394 Hz in the solid state. (Figure S13, ESI).<sup>35</sup> For the sake of completeness, the stereogenic nature of the phosphorus atoms needs to be considered leading to complex diastomeric mixtures in case of open chain 1D-polyphosphanes.<sup>36</sup> However, coplanar arrangement of the polyphosphane chain has been demonstrated for **4** further corroborated by single crystal XRD for short chain oligomers such as **7**. Owing to the presence of a bisecting mirror plane along the phosphorus chain, the resulting achiral *meso*-form is likely to be the reason for the relatively simple signal pattern observed for **4**, **5** and **6**.



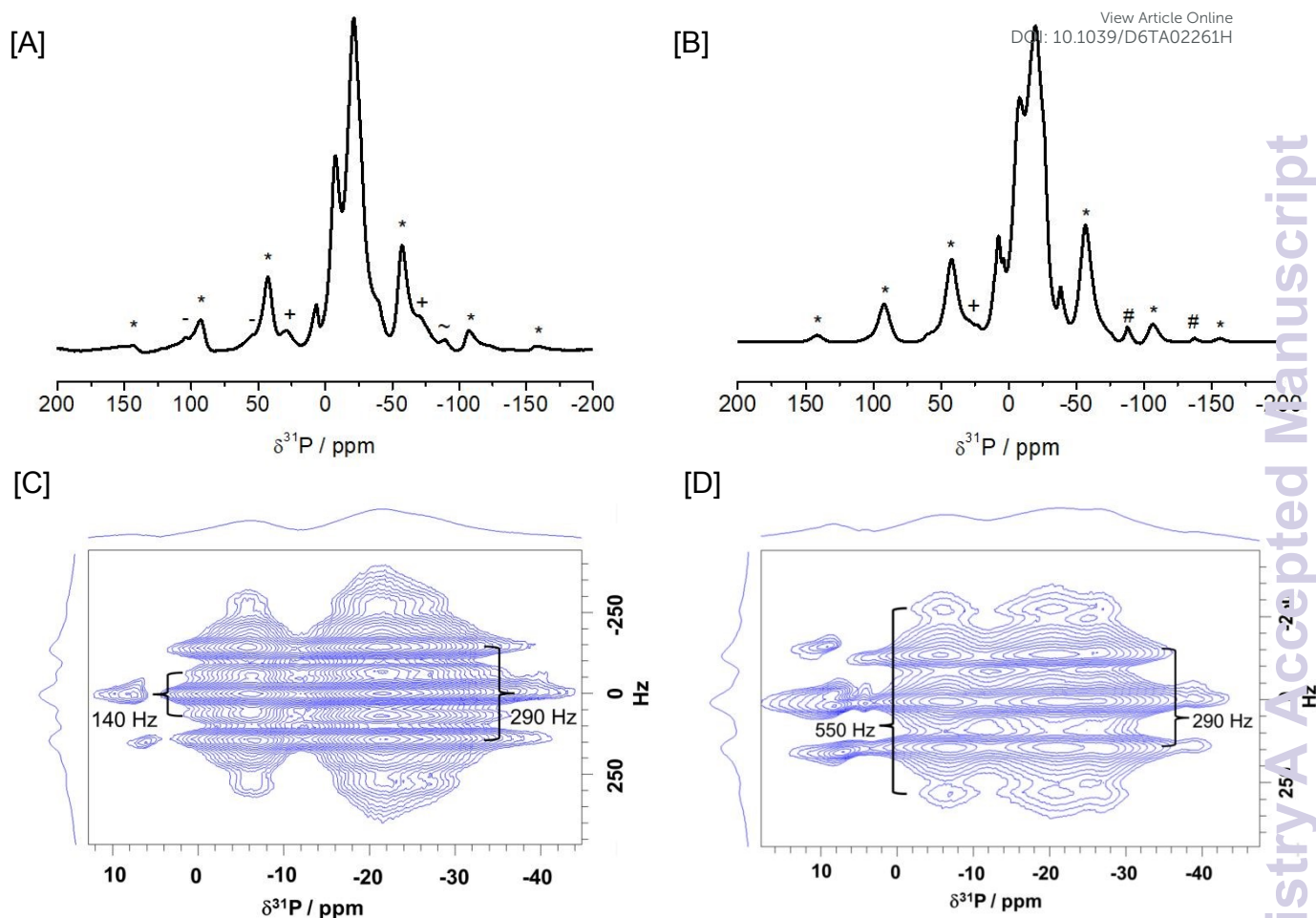


**Fig 3.**  $^1\text{H} \rightarrow ^{31}\text{P}$  CP MAS (measured at 14 T and 12 kHz spinning) of **5** (A) and **6** (B); ppm/Hz diagrams (featuring  $^{31}\text{P}$ - $^{31}\text{P}$  couplings) of **5** (C) and **6** (D), where spinning sidebands are marked with asterisks, plus, minus and tilde.

The subtle difference between these three polymers lies mainly in their terminal groups, with **4** featuring two *tert*-butyl groups as termination, **5** being a closed loop without terminal groups, and **6** carrying either *tert*-butyl or H at the terminal positions. One might speculate that the partial H-termination in **6** is rather a result of the presence of the  $>\text{P}-\text{H}$  unit in the precursor than of isobutene elimination from a  $>\text{P}-t\text{Bu}$  unit, since otherwise polymer **4** would contain  $>\text{P}-\text{H}$  units as well, which is not the case. Owing to the low reactivity of the solvents used in the extraction of by-products, alteration of these functionalities during the purification process is highly unlikely.

To probe the presence of H atoms on terminal P-atoms,  $^{31}\text{P}$  sostapt NMR experiments in the solid state were performed for polymer **6**. The spectra (Figure S18, ESI) were recorded individually and consecutively with and without applying  $^1\text{H}$  pulse power during inversion of  $^{31}\text{P}$  with a  $180^\circ$  pulse. By switching all  $^{31}\text{P}$  nuclei, other than those coupled directly to  $^1\text{H}$ , the signal resulting from the P atom resonating at about  $\delta$  -26.5 ppm shows negative amplitude, indicative for H-containing terminal P atoms. These interpretations are further consistent with the  $^1\text{H} \rightarrow ^{13}\text{C}$  CP MAS NMR spectrum of **6** featuring a weak intensity signal at  $\delta$  ca. 31 ppm, which can be assigned to residual *tert*-butyl as part of the end group (Figure S14, ESI). Unfortunately, the distortion of the signal intensity encountered during  $^1\text{H} \rightarrow \text{X}$  cross polarization precludes signal integration to quantify the abundance of the structural units. To get independent information on the ratio of end group vs. main chain units in **6**, CHN elemental analyses from two independently synthesized samples have been performed. As average values over several



samples in each case, best agreement has been obtained assuming two distinct compositions of ca.  ${}^t\text{Bu}-[\text{Fe}(\text{C}_5\text{H}_4\text{P})_2]_{86-95}\text{-H}$  and  ${}^t\text{Bu}-[\text{Fe}(\text{C}_5\text{H}_4\text{P})_2]_{608-2536}\text{-H}$ , indicating slightly and moderately longer chain length, as compared to **4**.<sup>13</sup> Compound **6** is stable and does not show any significant change upon further heating up to ca. 400 °C, as confirmed by elemental analysis. The constitutional similarity of **4**, **5** and **6** was further corroborated by vibrational spectroscopy, where comparison of the IR spectra of **4**,<sup>13</sup> **5**,<sup>15</sup> and **6** (Figure S19, ESI), in all cases show three strong and one medium strong signals in the range of  $\nu$  810-815  $\text{cm}^{-1}$ , 1022-1025  $\text{cm}^{-1}$ , and 1152-1158  $\text{cm}^{-1}$  for out of plane  $\text{C}^{\text{Cp}}\text{-H}$  bending, ring breathing, and asymmetric ring breathing of  $\text{C}^{\text{Cp}}\text{-C}^{\text{Cp}}$ , respectively in order.<sup>37, 38</sup> Stretching vibrations for the Cp-P bond are generally observed in the region of 1000–1100  $\text{cm}^{-1}$ , often overlapping with the Cp ring breathing modes.<sup>39</sup> In order to explore the electronic excitation of these polymeric materials, UV-Vis measurements were performed. In contrast to the parent ferrocene, which is known to exhibit two distinct absorption bands in the visible range, at 322 nm with a very low intensity and at 442 nm with high intensity,<sup>40</sup> polymers **4**, **5** and **6** feature much broader absorption bands in the solid state with almost equal intensities for the two previously mentioned absorptions (Figure 4). Moreover, the band at ca. 440 nm shows an intense shoulder above 500 nm which is more red shifted and intense for **5** and **6** than for **4**. In addition, these absorptions tail off still having significant intensities at wavelengths above 600 nm which are most pronounced for **6** followed by **5** and **4**. For the parent ferrocene, the bands at 440 nm with a weak shoulder at 528 nm have been assigned to dipole forbidden transitions which gain oscillator strength via vibronic coupling.<sup>41</sup> In line with this, in substituted ferrocenes the intensity of the latter increases and is shifted to longer wavelengths.<sup>40</sup> In the same vein, the higher energy transition at 322 nm has been reported to gain intensity upon mono- or disubstitution at ferrocene's Cp-rings but to lose intensity upon further substitution. In line with these findings, the high intensities and red shifted absorptions of **4**, **5** and **6** in the high energy region at ca. 325 nm are consistent with electronic modification of the Cp-ligands. The remarkable intensity gain for the absorption shoulder above 500 nm for **4**, **5** and **6**, most likely is a consequence of vibronic coupling as previously mentioned. To gain insight into this phenomenon, we performed DFT calculations on oligomeric model systems. Investigation of the frontier molecular orbitals indicate significant interaction of the lone pairs at phosphorus in the ferrocenylene bridged all-trans oriented phosphorus chain (Figure S25). In consequence, the HOMO-LUMO gap significantly decreases in agreement with the observed red-shifted absorption in the UV-Vis region outlined above. The observed red-shifted absorption maxima and the spectral tail extending into the visible region is in agreement with the TD-DFT calculations on the model oligomeric system, which indicate several excited states with low oscillator strength above 450 nm. It needs to be noted, that the pronounced absorption features at long wavelength are significantly red-shifted compared with saturated low-molecular phosphanylferrocenes, such as compound **1**, for which the solid-state UV-Vis absorption spectrum was measured at identical conditions for comparison (Figure S26). Interestingly, the absorption of **4**, **5** and **6** above 500 nm already comes close to the absorption wavelength reported for related unsaturated phosphanylferrocenes containing diphosphene units located at ca. 540 nm.<sup>42-46</sup>

Article Online  
DOI: 10.1039/D6TA02261H



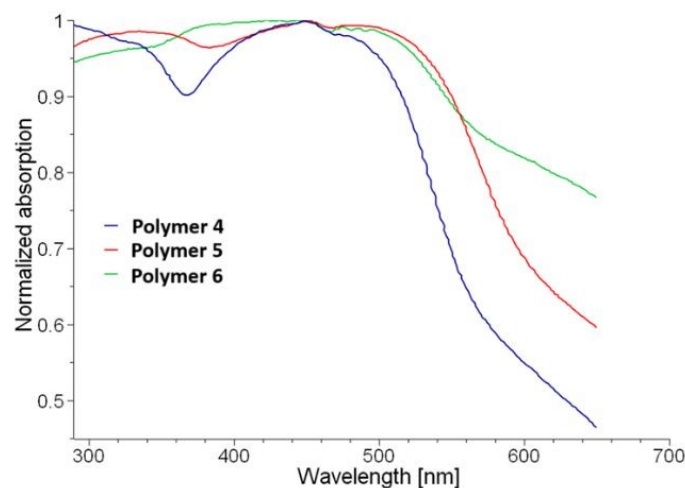
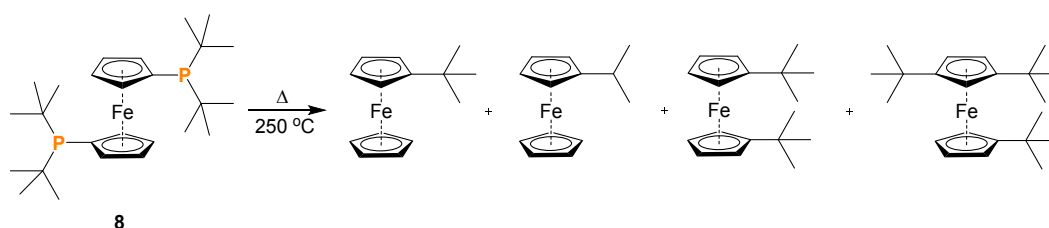


Fig 4. Solid state UV-Vis spectra of polymers 4, 5 and 6.

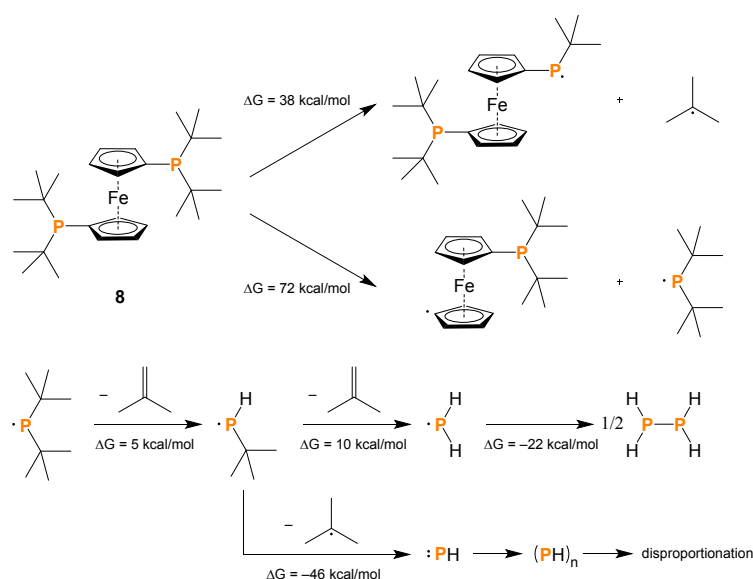


Scheme 4. Thermal reactions of  $\text{Fc}'(\text{P}^t\text{Bu}_2)_2$ .

To further understand the relevance of the P-H bond in the thermal conversion of **1** to **6**, we treated an analog in which the P-H unit is replaced by a second *tert*-butyl group, namely  $\text{Fc}'(\text{P}^t\text{Bu}_2)_2$  under identical conditions in a sealed ampule at 250 °C. However, to our surprise, the reaction proceeded via an uncontrolled P-C bond cleavage, where phosphorus-free  $\text{Fc}'(\text{tBu})$  and  $\text{tBu-Bu}$  were obtained as major products, along with  $\text{Fc}'\text{Pr}$ ,  $1,1'\text{-Fc}'(\text{tBu})_2$ , and  $1,3,1'\text{-Fc}'(\text{tBu})_3$ , in trace amounts (Scheme 4; Figures S23 and S24, ESI). This result has further been corroborated with MALDI MS, whereas no notable polymeric material could be recovered from this reaction. Moreover, the phosphorus content has been entirely transferred to the volatile by-products indicating a preferred cleavage of the P-C bond to the ferrocene in this particular case.

In order to understand the reactivity of the two different systems, DFT calculations were performed. Several possible reaction pathways, intermediates, and side products were considered (more details in the ESI). In view of the harsh reaction conditions, homolytic P-C bond cleavage is proposed as the initial step (Schemes S1 and S3, ESI File). The cleavage of the P-C(*t*Bu) bond is more favourable ( $\Delta G = 46$  kcal/mol for **1**, and  $\Delta G = 38$  kcal/mol for **8**, Scheme S1, ESI File) in both cases than the respective cleavage between the ferrocene unit and the phosphorus moiety ( $\Delta G = 77$  kcal/mol for **1**, and  $\Delta G = 69$  kcal/mol for **8**, Scheme S2, ESI File). Although both P-C(*t*Bu) and P-Cp cleavages are favorable for **8**, the observed reaction pathways contrasted our theoretical findings. Furthermore, considering the possible subsequent reactions, no significant differences in Gibbs free energy were observed among the pathways (Scheme S3), suggesting that the presence of the two *tert*-butyl groups may influence the reaction in other unprecedented ways. A possible explanation could be the availability of the eclipsed geometry, promoting intramolecular radical transfer and the formation of P-P-bonded products. In case of **8**, the eclipsed geometry is likely less favourable, allowing alternative reaction pathways to dominate. The considered reaction paths (Scheme 5) result in the formation of volatile phosphorus-containing by-products (e.g.  $\text{PH}_3$ ), which is consistent with the experiments, as no phosphorus-containing solid products were spectroscopically found when starting from precursor **8**.





**Scheme 5.** Thermodynamic profile of the thermal decomposition pathways of  $\text{Fc}'(\text{P}^t\text{Bu}_2)_2$  and its fragments computed at  $\omega\text{B97X-D/6-311+g}^{**}$  level of theory.

Comparing the overall synthetic strategies to such metallopolymers, it needs to be pointed out, that using compound **1** as the direct precursor as reported here is significantly more efficient and atom-economic than the previously published approach to **4**, where the actual precursor **2** likewise needs to be prepared from **1** in a multistep reaction involving metalation with *n*-butyl lithium and oxidative coupling to [2]ferrocenophane **2**. Therefore, these latter additional steps can be saved by using **1** as direct precursor to **6**. Otherwise, the energy requirements, reaction times and yields are almost identical in the thermolytic reactions to **4** and **6**.

### 3. Experimental

#### 3.1. General methodology

All manipulations were performed under argon atmosphere unless mentioned otherwise. Prior to use, the glassware was dried in drying oven under 120 °C. Solvents were distilled over drying agents, prescribed in CRC Handbook of chemistry and subsequently stored under argon atmosphere over 4 Å molecular sieves. Solvents for column chromatography and aqueous workups were used (analytical grade supplied by VWR and Alfa-Aesar) without further purification. NMR solvents (purchased from Deutero) were degassed via a few cycles of freeze, pump and thaw, and finally stored over 3 Å molecular sieves under Argon atmosphere. Reagents and chemicals were purchased from commercial suppliers (Sigma-Aldrich, ABCR, Alfa-Aesar) and used as received.  $\text{Fc}'(\text{P}^t\text{BuH})_2$  and polymers **4** and **5** were synthesized by following a published procedure.<sup>13, 15, 31</sup>

All solution-phase NMR spectra were measured on Jeol JNM-ECZL500, Varian 500VNMRS and Varian MR-400 spectrometers at 25 °C. Chemical shifts were referenced to residual protic impurities in the solvent ( $^1\text{H}$ ) or the deuterated solvent ( $^{13}\text{C}$ ) and reported relative to external  $\text{SiMe}_4$  ( $^1\text{H}$ ,  $^{13}\text{C}$ ). The signals, resulting from the residual nondeuterated NMR solvents, were referenced as indicated in the literature.<sup>47</sup> NMR Spectra of heteronuclei were referenced using the  $\Xi$ -scale following IUPAC recommendations with  $\text{H}_3\text{PO}_4$  (85%) ( $^{31}\text{P}$ ) as secondary references.<sup>48</sup>

All solid-state NMR measurements were performed on a Bruker Avance III HD 600 MHz spectrometer employing a 4 mm broad band H/X probe. Samples were packed into  $\text{ZrO}_2$  rotors. All spectra were recorded at 14 T, which leads to frequencies of 150.92 MHz for  $^{13}\text{C}$ , 242.93 MHz for  $^{31}\text{P}$  and 600.12 MHz for  $^1\text{H}$  respectively, at room temperature with a MAS spinning frequency of 8, 10 or 12 kHz as indicated in the figure captions. The CP MAS sequence was used with a linear 50-100 ramp on  $^1\text{H}$  and a contact time of 3.5 ms



for  $^{31}\text{P}$  and 2 ms for  $^{13}\text{C}$ . A  $\pi/2$  excitation pulse of 2.5  $\mu\text{s}$  was applied on  $^1\text{H}$ . TPPM15 broadband decoupling was applied during data acquisition.<sup>49, 50</sup> A recycle delay of 1 or 3 s, respectively, was used for all spectra.  $^{31}\text{P}$  spectra were recorded with 1024 and 256 scans and  $^{13}\text{C}$  spectra with 2028 scans, respectively. As a reference  $\text{H}_3\text{PO}_4$  (0 ppm) was used for  $^{31}\text{P}$ , and TMS (0 ppm) was used for  $^{13}\text{C}$ .  $^{31}\text{P}$  J-resolved spectra were recorded according to reference 35 establishing  $^{31}\text{P}$  polarization by means of CP with the parameters described above.<sup>35</sup> This was followed by a rotor synchronized  $\pi$  pulse ( $n=1, 2, \dots$ ) of 5  $\mu\text{s}$  on  $^{31}\text{P}$  and recording the spin echo. The  $^{31}\text{P}$  sostapt experiments were recorded at 12 kHz spinning employing the pulse sequence introduced by Lesage et al.<sup>51</sup> which is implemented in the Bruker Topspin 3.2 software package. Parameters for CP were used as described above. The  $\pi$  pulses were set to 5  $\mu\text{s}$  in the sequence. Homonuclear  $^1\text{H}$ - $^1\text{H}$  decoupling during the evolution time  $\tau$  was performed employing frequency switched Lee-Goldburg (FSLG).<sup>52</sup>

MALDI measurements were performed with Ultraflex der Firma Bruker Daltonics instruments using samples dissolved in HPLC-quality solvents. Elemental analyses were performed without using any external oxidizer in an EA 3000 Elemental Analyzer (EuroVector). Infrared spectra recorded for the neat substances were obtained using a Bruker Alpha Platinum ATR spectrometer, and Opus 6.5 (from Bruker Optics) was used for analysing the data. Strong, medium strong and weak peaks for these species were denoted as s, m and w, respectively. UV-Vis spectra were measured with the Hamamatsu C11347 system in solid state and for the refinement of data, OriginPro was used.

### 3.2. Solid-state NMR Characterization of polymer 5

Polymer **5** was synthesized by following a previously published procedure.<sup>15</sup>  $^{13}\text{C}$  CP MAS NMR  $\delta$  [ppm]: 79 and 73 ( $\text{C}^{\text{CP}}$ ) (Figure S8, ESI).  $^{31}\text{P}$  CP MAS NMR  $\delta$  [ppm]: 8, -8, -20 and -38 ppm (Figures S9 and S10, ESI).

### 3.3. Thermal oligo- and polymerization of 1 and synthesis of 6

100 mg of compound **1** was taken in a glass-vial and sealed under a vacuum of  $10^{-3}$  mbar, before keeping it at 250  $^\circ\text{C}$  for 4h. After cooling the vials down at room temperature, the inner soluble substances were dissolved in  $\text{C}_6\text{D}_6$ .  $^1\text{H}$  NMR ( $\text{C}_6\text{D}_6$ )  $\delta$  [ppm]: 0.87 (d,  $(\text{CH}_3)_3\text{CH}$ ,  $J = 7$  Hz from  $\text{Me}_3\text{CH}$ ), and 1.63 (dh,  $(\text{CH}_3)_3\text{CH}$ ,  $J = 13, 7$  Hz from  $\text{Me}_3\text{CH}$ ) (Figure S1, ESI).  $^{13}\text{C}$  NMR ( $\text{C}_6\text{D}_6$ )  $\delta$  [ppm]: 24.78 (s,  $(\text{CH}_3)_3\text{CH}$  from  $\text{Me}_3\text{CH}$ ) (Figure S2, ESI).  $^{31}\text{P}$  NMR ( $\text{C}_6\text{D}_6$ )  $\delta$  [ppm]: 39.09 (s,  $\text{Fc}'_2\text{P}_2$  from **3**), 20.43 (bm,  $(^t\text{BuP})_2[2]\text{FCP}$  from **2**), 3.60 (m,  $^t\text{BuP-P}$  from **7**), -26.12 (ddq,  $J = 206, 24, 12$  Hz from  $\text{Fc}'(\text{P}^t\text{BuH})_2$ ), -27.14 (d,  $J = 207$  Hz from  $\text{FcP}^t\text{BuH}$ ), -41.36 (m,  $^t\text{BuP-P}$  from **7**), and -80.29 (dddd,  $J = 198.5, 174.9, 23.7, 11.8$  Hz from  $^t\text{BuPH}_2$ ) (Figure S3, ESI).  $^{31}\text{P}$   $\{^1\text{H}\}$  NMR ( $\text{C}_6\text{D}_6$ )  $\delta$  [ppm]: 39.10 (s,  $\text{Fc}'_2\text{P}_2$  from **3**), 20.43 (s,  $(^t\text{BuP})_2[2]\text{FCP}$  from **2**), 3.57 (m,  $^t\text{BuP-P}$  from **7**), -26.64 (s from  $\text{FcP}^t\text{BuH}$ ), -27.08 (d,  $J = 94$  Hz from **1**), -41.64 (m,  $^t\text{BuP-P}$  from **7**), and -80.31 (s from  $^t\text{BuPH}_2$ ) (Figure 2). Molecular ion peaks for compounds **2**, **3**, and **7** have appeared at  $m/z$  360.185 (calcd. value 360.199), 491.931 (calcd. value 491.933), and 606.049 (calcd. value 606.165), respectively (Figures S5-S7, ESI).

After washing all the soluble materials with toluene ( $3 \times 10$  ml) and pentane ( $3 \times 10$  ml), the residual solid materials (**6**) were kept under a vacuum  $10^{-3}$  mbar, before characterizing via solid-state NMR measurements.  $^{13}\text{C}$  NMR (Solid-state)  $\delta$  [ppm]: 79 and 73 ( $\text{C}^{\text{CP}}$ ), 31 ( $^t\text{Bu}$ ) (Figure S14, ESI).  $^{31}\text{P}$  NMR (Solid-state)  $\delta$  [ppm]: 8, -8, -20 and -38 ppm (Figures S15 and S16, ESI). Anal. Calcd. for  $[\text{C}_{10}\text{H}_8\text{FeP}_2]_n$  (neglecting the terminal groups): C, 48.83; H, 3.28. Found: C, 48.92; H, 3.31 and C, 48.84; H, 3.28 for two parallelly performed identical polymerization reaction. Closer inspection taking terminal *tert*-butyl and H end groups into account indicates the molecular formula as  $[\text{C}_4\text{H}_9]-[\text{C}_{10}\text{H}_8\text{FeP}_2]_{86-95}-\text{H}$  (where  $\text{C}_4\text{H}_9 = ^t\text{Bu}$ ) from the first reaction, based on the average of samples from four consecutively measured elemental composition: C, 48.92; H, 3.31 (SD 0.07, SEM 0.02), where Anal. Calcd. For  $[\text{C}_4\text{H}_9]-[\text{C}_{10}\text{H}_8\text{FeP}_2]_{86-95}-\text{H}$ : C, 48.92; H, 3.31. On the other hand, the molecular formula could be found



as  $[\text{C}_4\text{H}_9]\text{-}[\text{C}_{10}\text{H}_8\text{FeP}_2]_{608-2536}\text{-H}$  from the second reaction, based on the average of samples from four consecutively measured elemental composition: C, 48.84; H, 3.28 (SD 0.03, SEM 0.04), where Anal. Calcd. For  $[\text{C}_{10}\text{H}_8\text{FeP}_2]_{86-95}[\text{C}_4\text{H}_9]\text{H}$ : C, 48.84; H, 3.28. IR (ATR)  $\nu$ : 810 (s, out of plane  $\text{C}^{\text{Cp}}\text{-H}$  bend), 848 (m, out of plane  $\text{C}^{\text{Cp}}\text{-C}^{\text{Cp}}$  bend), 892 (m, out of plane  $\text{C}^{\text{Cp}}\text{-C}^{\text{Cp}}$  bend), 1024 (s, ring breathing), 1157 (s, asymmetric ring breathing), 1363, (w, in-plane skeletal  $\text{C}^{\text{Cp}}\text{-C}^{\text{Cp}}$  vibration), and 1387 (m, in-plane skeletal  $\text{C}^{\text{Cp}}\text{-C}^{\text{Cp}}$  vibration) (Figure S19, ESI).

### 3.4. Thermal oligo- and polymerization of $\text{Fc}'(\text{P}^t\text{Bu}_2)_2$

100 mg of compound  $\text{Fc}'(\text{P}^t\text{Bu}_2)_2$  was taken in a glass-vial and sealed under a vacuum of  $10^{-3}$  mbar, before keeping it at 250 °C for 4h. The crude product was dissolved in  $\text{C}_6\text{D}_6$  before characterization with various methods.  $^1\text{H}$  NMR ( $\text{C}_6\text{D}_6$ )  $\delta$  [ppm]: 0.87 (d,  $J = 7$  Hz,  $\text{Fc-C}(\text{CH}_3)_3$  of  $\text{Fc}'(\text{tBu})$ ), 1.20 (s,  $(\text{CH}_3)_3\text{C-C}(\text{CH}_3)_3$ ), 3.92 (pst,  $\beta\text{-H}$  of  $\text{Cp}^{\text{tBu}}$  of  $\text{Fc}'(\text{tBu})$ ), 3.96 (pst,  $\alpha\text{-H}$  of  $\text{Cp}^{\text{tBu}}$  of  $\text{Fc}'(\text{tBu})$ ), 4.01 (Ferrocene) and 4.04 (s,  $\text{C}_5\text{H}_5$  of  $\text{Fc}'(\text{tBu})$ ) (Figure S20, ESI).  $^{13}\text{C}$  NMR ( $\text{C}_6\text{D}_6$ )  $\delta$  [ppm]: 24.79 (s,  $(\text{CH}_3)_3\text{C-C}(\text{CH}_3)_3$ ), 31.59 (s,  $\text{Fc-C}(\text{CH}_3)_3$  of  $\text{Fc}'(\text{tBu})$ ), 65.26 (s,  $\beta\text{-C}$  of  $\text{Cp}^{\text{tBu}}$  of  $\text{Fc}'(\text{tBu})$ ), 67.22 (s,  $\alpha\text{-C}$  of  $\text{Cp}^{\text{tBu}}$  of  $\text{Fc}'(\text{tBu})$ ), 68.23 (Ferrocene), and 68.46 (s,  $\text{C}_5\text{H}_5$  of  $\text{Fc}'(\text{tBu})$ ) (Figure S21, ESI). Molecular ion peaks for compounds  $\text{Fc}'\text{Pr}$ ,  $\text{Fc}'(\text{tBu})$ ,  $1,1'\text{-Fc}'(\text{tBu})_2$ , and  $1,3,1'\text{-Fc}'(\text{tBu})_3$  have appeared at  $m/z$  227.052 (M-1 cald. value 227.116), 242.075 (Cald. value 242.143), 298.137 (Cald. value 298.251), 354.200 (Cald. value 354.359), respectively (Figure S23, ESI). MALDI (HRMS) for  $\text{Fc}'(\text{tBu})$ :  $m/z$  242.0752 (Cald. value 242.0758) (Figures S23 and S24, ESI). NOTE: The empty baseline in  $^{31}\text{P}\{^1\text{H}\}$  NMR signifies the absence of any soluble P-containing species in the reaction mixture (Figure S22, ESI).

## 4. Theoretical Calculations

All calculations were performed by Gaussian 16 program package,<sup>53</sup> and Molden<sup>54</sup> was used to visualize the computed structures. Geometry optimizations were carried out at the  $\omega\text{B97X-D/6-311+g}^{**}$  level of theory. In some cases, the results were further validated by LNO-CCSD(T) single-point calculations performed with the MRCC program.<sup>55, 56</sup> Harmonic vibrational frequency analyses were performed on the fully optimized structures to verify their character; minima were confirmed by the presence of exclusively positive Hessian eigenvalues. Gibbs free energies were calculated at 298.15 K and atmospheric pressure using the computed harmonic frequencies.

## 5. Conclusions

In summary, we explored the question whether unstrained open-chain 1,1'-diphosphaferrocenes are capable of undergoing thermal dealkylation to metallopolymers or whether the ring strain of cyclic precursors currently in use are required. We found that comparable metallopolymers are accessible from unstrained open-chain precursors, but the substitution pattern decisively controls the product formation. Further indications for this reactivity was found in a multi-step reaction mechanism elucidated by DFT calculations, where the initial step is homolytic P-H and P-C( $\text{tBu}$ ) cleavages, forming dehydrogenated and dealkylated intermediates  $[(\eta^5\text{-C}_5\text{H}_4\text{-P}^t\text{Bu})\text{Fe}(\eta^5\text{-C}_5\text{H}_4\text{-PH}^t\text{Bu})]^\bullet$  and  $[(\eta^5\text{-C}_5\text{H}_4\text{-PH})\text{Fe}(\eta^5\text{-C}_5\text{H}_4\text{-P}^t\text{Bu}_2)]^\bullet$  from **1** and **8**, respectively. Due to the steric congestion between *tert*-butyl groups, species  $[(\eta^5\text{-C}_5\text{H}_4\text{-P}^t\text{Bu})\text{Fe}(\eta^5\text{-C}_5\text{H}_4\text{-PH}^t\text{Bu}_2)]^\bullet$  does not support eclipsed orientation on the ferrocene moiety, and consequently undergoes further thermal cleavages of P-C( $\text{tBu}$ ), followed by those of P-Cp bonds, giving rise to  $\text{Fc}'(\text{tBu})$  as identifiable major product with minor and trace impurities of other mono-, di-, and tri-substituted ferrocenes. Solid state  $^1\text{H}\rightarrow^{31}\text{P}$  CP MAS NMR turned out to be the most valuable technique for characterization of the polymer backbone via comparison of its characteristic NMR signature with closely related polymers. Indications for P-H termination have been obtained using  $^{31}\text{P}$  sostapt NMR experiments in the solid state. However, cross polarization precludes quantitative information on the relative abundance of structural units. Obviously, simple and robust precursors, **1** is air stable as neat substance,<sup>32</sup> will facilitate the accessibility of metallopolymers. Its direct use as precursor to metallopolymers avoids additional synthetic effort in preparing strained precursors from the



same starting compound. We are convinced that further examples of unstrained precursors with reactive element-carbon bonds will lead to their respective metallopolymer in the future.

Article Online  
DOI: 10.1039/D6TA02261H

### **Ulrich Schubert dedication**

The authors dedicate this work to Professor Dr Ulrich Schubert on the occasion of his 80th birthday in recognition of his exceptional scientific achievements and enduring impact in materials chemistry.

### **Authorship contribution statement**

**Subhayan Dey:** Investigation and conceptualization; **Balázs Szathmári:** Investigation; **Dennis Langgut:** Investigation; **Zsolt Kelemen:** Supervision and conceptualization; **Torsten Gutmann:** Supervision and conceptualization; **Rudolf Pietschnig:** Supervision and conceptualization.

### **Conflict of Interests**

The authors declare no conflict of interest.

### **Data availability**

The supporting data has been provided as part of the Supplementary information. Supplementary information: Figures S1-S26, NMR spectra, MS spectra, IR spectra, UV/vis spectra, and Kohn-Sham FMO; Schemes S1-S5, computational information on thermodynamic decomposition pathways. Geometries of computed structures have been provided as xyz-file.

### **Acknowledgement**

S.D. thanks Vellore Institute of Technology, Chennai Campus, India, for providing "VIT RGEMS SEED GRANT" (Sanction Order No. PH1/2024/SG2024001) for carrying out this research work. We thank Prof. Buntkowsky (TU Darmstadt) for generous allocation of measurement time-slots on his 600 MHz Bruker Avance III HD spectrometer. Dr. Hergen Breitzke is gratefully acknowledged for technical support of the solid-state NMR measurements. R.P. and S.D. are further grateful to the University of Kassel ZFF-program for their generous contribution in funding this research. Z.K. is grateful for the support of OTKA FK-145841 provided by the Hungarian National Research Development and Innovation Office.

### **References**

1. J. E. Mark, H. R. Allcock and R. West, *Inorganic polymers*, Prentice Hall, NJ, USA, 1992.
2. V. Chandrasekhar, *Inorganic and Organometallic Polymers*, Springer Berlin Heidelberg, Germany, 2005.
3. B. Toury and P. Miele, *J. Mat. Chem.*, 2004, **14**, 2609-2611.
4. R. Pietschnig, *Chem. Soc. Rev.*, 2016, **45**, 5216-5231.
5. V. Bellas and M. Rehahn, *Angew. Chem., Int. Ed.*, 2007, **46**, 5082-5104.
6. D. Löber, S. Dey, B. Kaban, F. Roesler, M. Maurer, H. Hillmer and R. Pietschnig, *Molecules*, 2020, **25**, 2438.
7. S. Vijayalakshmi, S. Dey and K. Rajendrakumar, *J. Macromol. Sci., Part A:Pure Appl. Chem.*, 2025, **63**, 1-18.
8. D. E. Herbert, U. F. Mayer and I. Manners, *Angew. Chem., Int. Ed.*, 2007, **46**, 5060-5081.
9. H. Bhattacharjee, S. Dey, J. Zhu, W. Sun and J. Muller, *Chem. Commun.*, 2018, **54**, 5562-5565.
10. E. Khozeimeh Sarbisheh, H. Bhattacharjee, M. P. T. Cao, J. Zhu and J. Müller, *Organometallics*, 2017, **36**, 614-621.
11. H. P. Withers, D. Seyferth, J. D. Fellmann, P. E. Garrou and S. Martin, *Organometallics*, 1982, **1**, 1283-1288.



12. R. Rulkens, A. J. Lough and I. Manners, *J. Am. Chem. Soc.*, 1994, **116**, 797-798.
13. S. Dey, D. Kargin, M. V. Höfler, B. Szathmári, C. Bruhn, T. Gutmann, Z. Kelemen and R. Pietschnig, *Polymer*, 2022, **242**, 124589.
14. Y. Tanimoto, Y. Ishizu, K. Kubo, K. Miyoshi and T. Mizuta, *J. Organomet. Chem.*, 2012, **713**, 80-88.
15. S. Dey, B. Szathmari, R. Franz, C. Bruhn, Z. Kelemen and R. Pietschnig, *Chem. Eur. J.*, 2024, **30**, e202400194.
16. C. T. Aitken, J. F. Harrod and E. Samuel, *J. Am. Chem. Soc.*, 1986, **108**, 4059-4066.
17. S. M. Katz, J. A. Reichl and D. H. Berry, *J. Am. Chem. Soc.*, 1998, **120**, 9844-9849.
18. T. Imori, V. Lu, H. Cai and T. D. Tilley, *J. Am. Chem. Soc.*, 1995, **117**, 9931-9940.
19. H. Dorn, J. M. Rodezno, B. Brunnhöfer, E. Rivard, J. A. Massey and I. Manners, *Macromolecules*, 2003, **36**, 291-297.
20. R. Zhang, J. E. Mark and A. R. Pinhas, *Macromolecules*, 2000, **33**, 3508-3510.
21. M. B. Reuter, D. M. Seth, D. R. Javier-Jiménez, E. J. Finfer, E. A. Beretta and R. Waterman, *Chem. Commun.*, 2023, **59**, 1258-1273.
22. R. J. Less, R. L. Melen and D. S. Wright, *RSC Adv.*, 2012, **2**, 2191-2199.
23. R. L. Melen, *Dalton Trans.*, 2013, **42**, 16449-16465.
24. W. J. Transue, A. Velian, M. Nava, C. García-Iriepa, M. Temprado and C. C. Cummins, *J. Am. Chem. Soc.*, 2017, **139**, 10822-10831.
25. V. Naseri, R. J. Less, R. E. Mulvey, M. McPartlin and D. S. Wright, *Chem. Commun.*, 2010, **46**, 5000-5002.
26. H. Schneider, D. Schmidt and U. Radius, *Chem. Commun.*, 2015, **51**, 10138-10141.
27. V. J. Eilrich and E. Hey-Hawkins, *Coord. Chem. Rev.*, 2021, **437**, 213749.
28. T. N. Hooper, A. S. Weller, N. A. Beattie and S. A. Macgregor, *Chem. Sci.*, 2016, **7**, 2414-2426.
29. D. Han, F. Anke, M. Trose and T. Beweries, *Coord. Chem. Rev.*, 2019, **380**, 260-286.
30. A. Schäfer, T. Jurca, J. Turner, J. R. Vance, K. Lee, V. A. Du, M. F. Haddow, G. R. Whittell and I. Manners, *Angew. Chem. Int. Ed.*, 2015, **54**, 4836-4841.
31. D. Kargin, Z. Kelemen, K. Krekic, M. Maurer, C. Bruhn, L. Nyulaszi and R. Pietschnig, *Dalton Trans.*, 2016, **45**, 2180-2189.
32. F. Horký, R. Franz, C. Bruhn and R. Pietschnig, *Chem. Eur. J.*, 2023, **29**, e202302518.
33. K. P. Barry and C. Nataro, *Inorg. Chim. Acta*, 2009, **362**, 2068-2070.
34. P. Kilian, A. M. Z. Slawin and J. D. Woollins, *Chem. Eur. J.*, 2003, **9**, 215-222.
35. A. Grünberg, X. Yeping, H. Breitzke and G. Buntkowsky, *Chem. Eur. J.*, 2010, **16**, 6993-6998.
36. R. Wolf, M. Finger, C. Limburg, A. C. Willis, S. B. Wild and E. Hey-Hawkins, *Dalton Trans.*, 2006, 831-837.
37. L. Phillips, A. R. Lacey and M. K. Cooper, *J. Chem. Soc., Dalton Trans.*, 1988, DOI: 10.1039/DT9880001383, 1383-1391.
38. T. P. Gerasimova and S. A. Katsyuba, *J. Organomet. Chem.*, 2015, **776**, 30-34.
39. V. Ivanovski, M. Bukleski, M. Madalska and E. Hey-Hawkins, *Vib. Spectrosc.*, 2013, **69**, 57-64.
40. A. Paul, R. Borrelli, H. Bouyanfif, S. Gottis and F. Sauvage, *ACS Omega*, 2019, **4**, 14780-14789.
41. U. Salzner, *J. Chem. Theory Comput.*, 2013, **9**, 4064-4073.
42. R. Pietschnig and E. Niecke, *Organometallics*, 1996, **15**, 891-893.
43. N. Nagahora, T. Sasamori, N. Takeda and N. Tokitoh, *Chem. Eur. J.*, 2004, **10**, 6146-6151.
44. C. Moser, M. Nieger and R. Pietschnig, *Organometallics*, 2006, **25**, 2667-2672.
45. N. Nagahora, T. Sasamori, Y. Watanabe, Y. Furukawa and N. Tokitoh, *Bull. Chem. Soc. Jpn.*, 2007, **80**, 1884-1900.
46. T. Sasamori, M. Sakagami, M. Niwa, H. Sakai, Y. Furukawa and N. Tokitoh, *Chem. Commun.*, 2012, **48**, 8562-8564.
47. G. R. Fulmer, A. J. M. Miller, N. H. Sherden, H. E. Gottlieb, A. Nudelman, B. M. Stoltz, J. E. Bercaw and K. I. Goldberg, *Organometallics*, 2010, **29**, 2176-2179.
48. R. K. Harris, E. D. Becker, S. M. C. d. Menezes, R. Goodfellow and P. Granger, *Pure Appl. Chem.*, 2001, **73**, 1795-1818.

View Article Online  
DOI: 10.1039/D6TA02261H

49. I. Scholz, P. Hodgkinson, B. H. Meier and M. Ernst, *J. Chem. Phys.*, 2009, **130**, 114510. [View Article Online](#)  
DOI: 10.1039/D6TA02261H
50. S. Dey, F. Roesler, M. V. Höfler, C. Bruhn, T. Gutmann and R. Pietschnig, *Eur. J. Inorg. Chem.*, 2021, **2022**, e202100939.
51. A. Lesage, S. Steuernagel and L. Emsley, *J. Am. Chem. Soc.*, 1998, **120**, 7095-7100.
52. B. J. van Rossum, H. Förster and H. J. M. de Groot, *J. Magn. Reson.*, 1997, **124**, 516-519.
53. M. J. Frisch, G. W. Trucks, H. B. Schlegel, G. E. Scuseria, M. A. Robb, J. R. Cheeseman, G. Scalmani, V. Barone, G. A. Petersson, H. Nakatsuji, X. Li, M. Caricato, A. V. Marenich, J. Bloino, B. G. Janesko, R. Gomperts, B. Mennucci, H. P. Hratchian, J. V. Ortiz, A. F. Izmaylov, J. L. Sonnenberg, Williams, F. Ding, F. Lipparini, F. Egidi, J. Goings, B. Peng, A. Petrone, T. Henderson, D. Ranasinghe, V. G. Zakrzewski, J. Gao, N. Rega, G. Zheng, W. Liang, M. Hada, M. Ehara, K. Toyota, R. Fukuda, J. Hasegawa, M. Ishida, T. Nakajima, Y. Honda, O. Kitao, H. Nakai, T. Vreven, K. Throssell, J. A. Montgomery Jr., J. E. Peralta, F. Ogliaro, M. J. Bearpark, J. J. Heyd, E. N. Brothers, K. N. Kudin, V. N. Staroverov, T. A. Keith, R. Kobayashi, J. Normand, K. Raghavachari, A. P. Rendell, J. C. Burant, S. S. Iyengar, J. Tomasi, M. Cossi, J. M. Millam, M. Klene, C. Adamo, R. Cammi, J. W. Ochterski, R. L. Martin, K. Morokuma, O. Farkas, J. B. Foresman and D. J. Fox, *Gaussian 16 Rev. C.01*, Wallingford, CT, 2016.
54. N. M. O'boyle, A. L. Tenderholt and K. M. Langner, *J. Comp. Chem.*, 2008, **29**, 839-845.
55. D. Mester, P. R. Nagy, J. Csóka, L. Gyevi-Nagy, P. B. Szabó, R. A. Horváth, K. Petrov, B. Hégyely, B. Ladóczki, G. Samu, B. D. Lőrincz and M. Kállay, *J. Phys. Chem. A*, 2025, **129**, 2086-2107.
56. M. Kállay, P. R. Nagy, D. Mester, L. Gyevi-Nagy, J. Csóka, P. B. Szabó, Z. Rolik, G. Samu, B. Hégyely, B. Ladóczki, K. Petrov, J. Csontos, Á. Ganyecz, I. Ladjánszki, L. Szegedy, M. Farkas, P. D. Mezei, R. A. Horváth and B. D. Lőrincz., MRCC, a quantum chemical program suite, [www.mrcc.hu](http://www.mrcc.hu)).



### Data availability statement

View Article Online  
DOI: 10.1039/D6TA02261H

The supporting data has been provided as part of the Supplementary information. Supplementary information: Figures S1-S25, NMR spectra, MS spectra, IR spectra and UV/vis spectra, Schemes S1-S4, computational information on thermodynamic decomposition pathways. Geometries of computed structures have been provided as xyz-file.

